Journal of Groundwater Science and Engineering
ISSN 2305-7068
Indexed by ESCI CABI CSA
Scopus GeoRef AJ CNKI

Identified the hydrochemical and the sulfur cycle process in subsidence area of Pingyu mining area using multi-isotopes combined with hydrochemistry methods

Hui-Meng Su, Fa-Wang Zhang, Jing-Yu Hu, Jin-Feng Lei, Wei Zuo, Bo Yang, Yu-Hua Liu

Citation:
Su HM, Zhang FW, Hu JY, *et al*. 2024. Identified the hydrochemical and the sulfur cycle process in subsidence area of Pingyu mining area using multi-isotopes combined with hydrochemistry methods. Journal of Groundwater Science and Engineering, 12(1): 62-77.

View online: https://doi.org/10.26599/JGSE.2024.9280006

Journal of Groundwater Science and Engineering 12(2024) 62–77

Journal homepage: http://gwse.iheg.org.cn

Original Article

Identified the hydrochemical and the sulfur cycle process in subsidence area of Pingyu mining area using multi-isotopes combined with hydrochemistry methods

Hui-Meng Su[1], Fa-Wang Zhang[1,2*], Jing-Yu Hu[3], Jin-Feng Lei[3], Wei Zuo[4,5], Bo Yang[4,5], Yu-Hua Liu[4,5]

[1] *School of Environmental Studies*, *China University of Geosciences*, *Wuhan* 430074, *China*.
[2] *Center for Hydrogeology and Environmental Geology*, *China Geological Survey*, *Baoding* 071051, *Hebei Province*, *China*.
[3] *Henan Branch*, *China South-to-North Water Diversion Middle Route Corporation Limited*, *Zhengzhou* 450046, *China*.
[4] *The Fifth Geological Survey Institute*, *Henan Provincial Bureau of Geology and Mineral Resources*, *Zhengzhou* 450012, *China*.
[5] *Natural Resources Science and Technology Innovation Center of Henan Province (Research on Eco-Environmental Assessment and Restoration Technology)*, *Zhengzhou* 450012, *China*.

Abstract: Groundwater serves as an important water source for residents in and around mining areas. To achieve scientific planning and efficient utilization of water resources in mining areas, it is essential to figure out the chemical formation process and the ground water sulfur cycle that transpire after the coal mining activities. Based on studies of hydrochemistry and D,^{18}O-H_2O,^{34}S-SO_4 isotopes, this study applied principal component analysis, ion ratio and other methods in its attempts to reveal the hydrogeochemical action and sulfur cycle in the subsidence area of Pingyu mining area. The study discovered that, in the studied area, precipitation provides the major supply of groundwater and the main water chemistry effects are dominated by oxidation dissolution of sulfide minerals as well as the dissolution of carbonate and silicate rocks. The sulfate in groundwater primarily originates from oxidation and dissolution of sulfide minerals in coal-bearing strata and human activities. The mixed sulfate formed by the oxidation of sulfide minerals and by human activities continuously recharges the groundwater, promoting the dissolution of carbonate rock and silicate rock in the process.

Keywords: PCA; Ion ratio; Water chemistry; Sulfide minerals; Multi-isotopes; Subsidence area of mining area

Received: 15 Jun 2023/ Accepted: 15 Dec 2023/ Published: 15 Mar 2024

Introduction

Coal is an important basic energy source and raw material in China (Tao et al. 2022). However, the process of coal mining is bound to cause damage and impact to groundwater in mining areas (Zhang et al. 2021; Sahoo et al. 2020), especially in northern China, where karst water often submerges in the coal measures, and high-intensity concentrated coal mining will greatly damage the original aquifer structure in the mining area. Large amount of water drainage in mine crates will also lead to large-scale ground subsidence or collapse in and around the mining area (Su et al. 2018), which in turn will change the original groundwater flow characteristics and hydrogeochemical processes around the mining area (Cha et al. 2022; Acharya et al. 2020). Groundwater functions as an important water source for residential areas around mining areas in northern China, and excessive SO_4^{2-} will greatly increase the salinity of water bodies, causing serious effect on human health and local ecological balance (Qu et al. 2022). Therefore, it is of great significance to study the hydrochemistry and laws of sulfur cycle of groundwater

*Corresponding author: Fa-Wang Zhang, *E-mail address*: zhangfawang@karst.ac.cn

DOI: 10.26599/JGSE.2024.9280006

Su HM, Zhang FW, Hu JY, et al. 2024. Identified the hydrochemical and the sulfur cycle process in subsidence area of Pingyu mining area using multi-isotopes combined with hydrochemistry methods. Journal of Groundwater Science and Engineering, 12(1): 62-77.

around mining areas so as to scientifically utilize the groundwater and improve its quality around the mining area, .

Groundwater hydrochemistry in mining areas is mainly influenced by a combination of natural effects such as endowment conditions and water-rock interaction, and anthropogenic activities such as coal production and human living (Acharya et al. 2020; Rinder et al. 2020), and ion ratio is one of the methods commonly used to analyze the hydro chemical evolution of groundwater (Zhang et al. 2021). Stable isotopes are sensitive tracers for tracing the origin of water bodies and ion sources (Moya et al. 2016). Since D and ^{18}O-H_2O are important components of water molecules, the significant differences between D and ^{18}O-H_2O from varied sources have paved way for of hydrogen and oxygen isotopes to trace the source of groundwater (Ansari et al. 2020). Sulfate is hardly fractionated during its formation, so ^{34}S- SO_4 can be used as a characteristic chemical "fingerprint" to demonstrate the sulfur cycling and the study of the migration and transformation process of sulfate can effectively analyze the sulfur cycling law in water bodies (Banks et al. 2020). In recent years, many Chinese and international scholars have applied a variety of methods combined with isotopes analysis to examine the sulfur cycle of groundwater in mining areas and other issues. For example, David et al. (2023) interpreted the solute and sulfur cycle in mine water by combining the stable isotope composition of D, ^{18}O-H_2O and ^{34}S-SO_4 in water from abandoned and flooded mines with data of drilling holes and hydrochemistry. Wang et al. (2022) and Mao et al. (2022) respectively used the self-organization mapping function of artificial intelligence to analyze isotope and hydro chemical data of the mining area, studying the changes of hydro chemical characteristics before and after mining, which revealed the mechanism of hydrogeochemical evolution in the multi-layer aquifer before and after mining, as well as the sulfur cycle process of the mining area. Huang et al. (2023) employed multi-isotope and hydro chemical analysis to investigate the source of sulfate and the sulfur cycling process in groundwater in North-China-type coal mines surrounding area . Previous researches have, mostly focused on the sulfur cycle of groundwater in mining areas by means of hydrochemistry and multi-isotope analysis (Ágnes et al. 2022; Ren et al. 2021; Zheng et al. 2019), while little paid attention to the subsidence area around the mining area caused by mining.

Located in Xuchang City, Henan Province, the Pingyu mining area used to be in a region rich in groundwater resources with developed springs and surface rivers. In May 2010, the first crate of Pingyu Mine started to evacuate karst water on a large scale. After 11 years of mining, the karst water level has decreased from 120–130 m in May 2010 to 210–180 m in July 2021, while a number of rivers in the area have been cut off, Happiness Lake and other natural spring groups, which were originally formed by karst water recharge, have also dried up one after another. Apart from the annual supply from the South-to-North Water Diversion Project, there is no other drinkable surface water source in the questioned area. Rural areas, as well as industrial and agricultural production is highly dependent on the mixed mining of pore water and karst water. The large amount of groundwater pumping has led to the successive occurrence of ground subsidence with a total area of about 19 km^2 around the mining area, where some channels of the South-to-North Water Diversion Center Line have also suffered impacts of ground subsidence. The cumulative amount of ground subsidence reached 60.63–155.29 mm, with a continuous increase rate of 10–20 mm/a, seriously threatening the safe and stable operation of the channels in the long run (Su et al. 2023; Pan et al. 2011). Previous studies on this area have mainly focused on groundwater flow characteristics and karst water recharge sources (Zhang, 2017; Tang, 2011; Pan et al. 2011), but there has been no research related to groundwater environment. Therefore, in order to ensure the water safety for residents in and around the mining area, and to enhance the utilization rate of water resources around the mine, there is an urgent need to study the hydrochemistry and sulfur cycling process of groundwater (pore water and karst water alike) after large-scale evacuation of karst water in the ground subsidence area around the mine. In this study, a combination of multi-isotope, hydrochemistry and principal component analysis is applied to gain insights of the hydro chemical evolution of groundwater and to reveal the sulfur cycling mechanism in the ground subsidence zone formed by mining hydrophobicity. The main objectives of this study are as follows: 1) to describe the hydro chemical characteristics and major hydrogeochemical processes in the subsidence zone of Pingyu Mine through principal component analysis and ion ratio analysis; 2) to analyze the groundwater and its sulfate sources in the subsidence zone of the mining area using D, ^{18}O-H_2O, ^{34}S- SO_4 multiple isotopes; 3) to elucidate the sulfur cycling mechanism in the subsidence zone under the influ-

ence of mining activities. This study aims to improve the understanding of groundwater evolution and sulfur cycling process in the subsidence zone of Pingyu Mine and provide scientific support for local groundwater management.

1 Study area

1.1 Natural features

The studied area is located in the northwest of Xuchang City, Henan Province, China. The overall landscape of the studied area leans from northwest towards southeast (Fig. 1). Except for the Guci Mountains in the north, other parts of the studied area are covered by the Quaternary alluvial plain. Pingyu mining area is located in the south of the studied area, covering a total area of 13.5 km^2. The studied area is exposed to continental monsoon climate, with an average annual temperature ranging from 13.0°C to 16.0°C, rainfall concentrated from July to September, and an average annual precipitation of 665 mm. The major rivers in the studied area are the Yinghe River and the Shiliang River, which belong to the Yinghe River system in the Huaihe River basin. Limited by topography, all the rivers in the studied area flow from northwest to southeast. are The middle route of the South-to-North Water Diversion Project functions as the main water conservancy facilities in this area, in addition to which are a number of drought relief reservoirs and subsidence lakes formed due to long-term coal mining activities around the mining area. is Densely populated and crowded with ore processing factories and machineryl processing factories, the studied area relies mainly on supply of groundwater and water from the South-to-North Water Diversion channel. Sewage, through underground pipeline networks, and the mine drainage processed by sedimentation treatment in the mining area are discharged into the neighboring natural rivers.

1.2 Geology

The tectonic unit of the studied area generally manifests a monoclinal structure, where Pingyu mining area is found in the northeast of the northern flank of Baisha syncline (Fig. 1). The exposed strata in the studied area consists of Songshan Group of Lower Proterozoic, Sinian System of Upper Proterozoic, Cambrian system of Lower Paleozoic, Carboniferous and Permian system of Upper Paleozoic, Paleogene system of Cenozoic, Neogene system and Quaternary system, among which Carboniferous-Permian system is the main

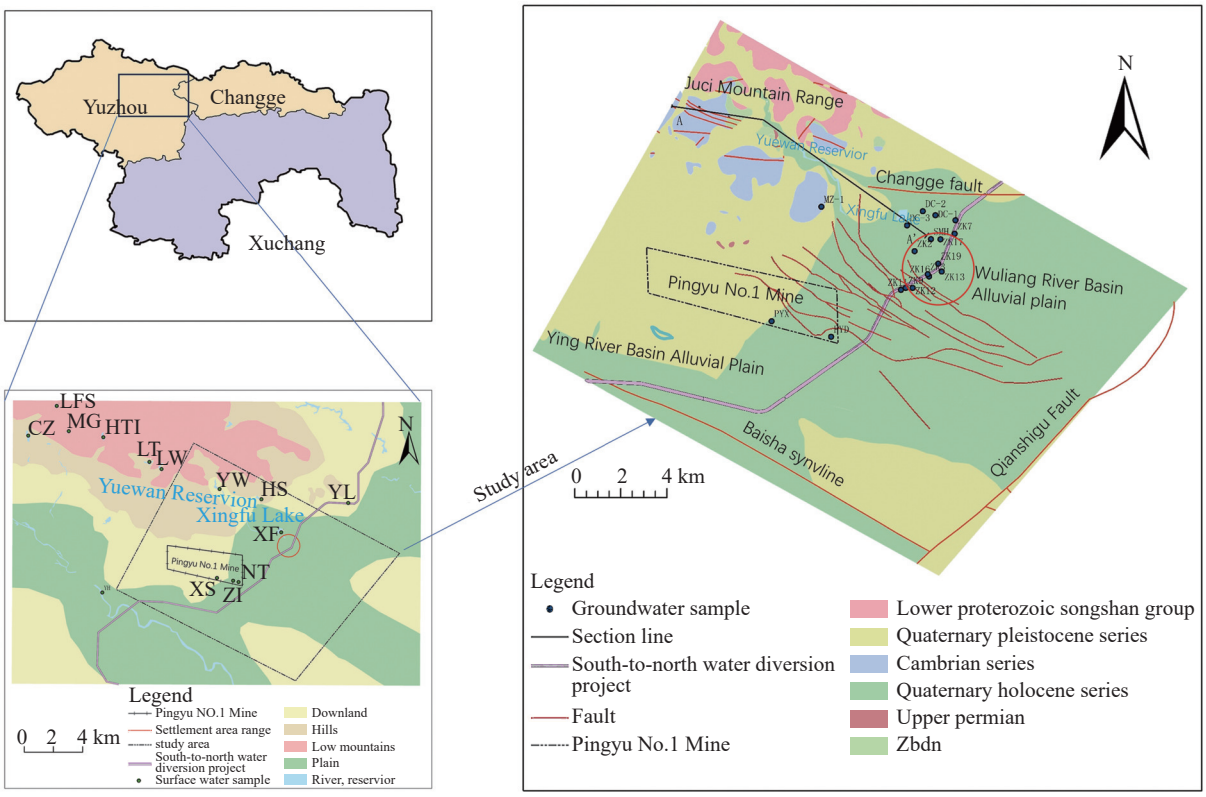

Fig. 1 Map of geological geomorphology and sampling points in the study area

coal-bearing strata, and 2_1 coal seam of Shanxi Formation of Lower Permian system is the exploitable coal seam in this area. The coal-bearing strata are rich in pyrite and other sulfide crystals, but contains no evaporite minerals such as gypsum. The northeastern part of the mining area is covered with folds in the east-west direction, accompanied by parallel fractures and a group of torsional fissures. Along the fractures are extrusion schisto-chemistry zones, crushing-influenced zones and fissure-intensive zones, which regulate the formation and distribution of karst water (Pan et al. 2011).

1.3 Hydrogeology

Except for the Guci Mountain area in the northern part of the research area, pore water is widely distributed in the Quaternary impact plain. The aquifer is composed of Neogene fluvial lacustrine sedimentary layer and Lower Pleistocene alluvial-lacustrine sedimentary layer, with the lithology of the Neogene fine sand, medium fine sand, coarse medium sand or sandstones, appear to be semiclastic, and with the mineral composition of quartz as dominant component. Pore water is replenished by atmospheric precipitation, surface water and lateral runoff from the west, with Yinghe River as the southern boundary of the discharge area and the line between unconsolidated strata and bedrock as the western part of the northern boundary, while the eastern part receives runoff recharge from the north. The lower interface of the pore water aquifer is located afore mountain, forming a water-repellent boundary by contacting sandstone and shale.

In the northwest and north part of the studied area bedrock and limestone belong to the exposed karst area are found exposed (Fig. 1), consisting of metamorphic rocks and intrusive rocks of the Proterozoic era, and of Paleozoic carbonates and clastic rocks. In the east and southeast direction, the area gradually falls under the cover of loose layers, and the burial depth gradually increases from more than 10 meters in the west to about 400 meters in the east. Previous borehole and geological data provided by predecessors (Pan et al. 2011) show that the karst water in the area is categorized as Cambrian limestone karst water with the main lithological compositions are dolomitic limestone and siliceous masses or bands. The karst water in the studied area is primarily supplied by atmospheric precipitation in the western mountain area (Pan et al. 2011). The karst water aquifer ends in the east with the former Shigu fault, with the Baisha syncline axis the southern boundary, both of which is water-repellent boundary, and its northern boundary is the Guci Mountains. Karst water runs off on steep slope from the western exposed karst area down to the east and southeast, gradually entering the areas where it is covered and then buried. The buried area finds its place between two layers of water-repellent boundaries, on is between the buried area and the upper sandstone, the other is the bottom interface of the limestone fromed by Cambrian sand shale.

Before the large-scale drainage of karst water in Pingyu Mining area, karst confined water in the thin carboniferous thin-bedded tuff and Cambrian thick-bedded tuff at the base of coal seam in the northern and northwestern mountain area in the mining area served as the major source of filling for mine water in Pingyu Mine. Karst water enters the coal mining face through karst fractures, fissures, faults, mining-induced fractures and poorly closed boreholes, threatening the safety of mine production. Besides, karst water also discharges naturally through the tectonic fractures in the northeastern part of the mine, where it supports and fills the loose strata and forms a cluster of karst springs (Fig. 2). For now, mine drainage in Pingyu Mine has completely altered the characteristics of local groundwater recharge and discharge. Although karst water in the northern and northwestern mountainous area is provided main supply of mine water in Pingyu mining area, the original natural discharge points of karst water has dried up one after another. Previously, the karst water supported and refilled the upper-layer pore water, while now the former has to receive cross-flow recharges from the latter (Su et al. 2023).

2 Data sources and test methods

2.1 Sample collection

Sampling principle: Taking into account both the types and lithology of aquifers in the studied area, drilling sampling constructions were carried out from July 2021 to August 2022 in areas showing relatively obvious influence of land subsidence (i.e. human gathering areas and important water conservancy facilities), collecting a total of 32 groups of groundwater and surface water samples of different aquifers (Fig. 1 for the locations of sampling spots).

In this study, a total of 14 groups of surface water samples were collected, including 2 groups of river water samples, 1 group of samples from

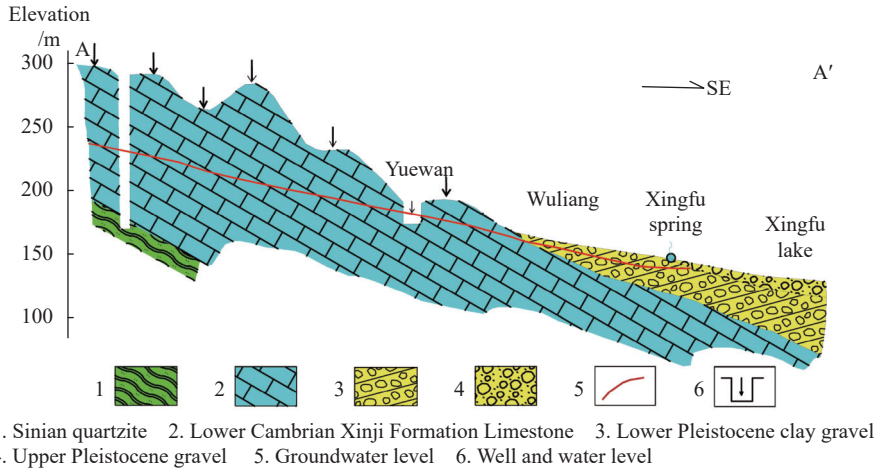

Fig. 2 Hydrogeological profile (2008) of the study area

the middle route channel of the South-to-North Water Diversion Project, 3 groups of subsidence lake water, 1 group of water from the Happiness Lake, and 7 groups of reservoir water. 15 groups of groundwater samples were collected, including 8 groups of pore water and 7 groups of karst water. For testing sulfur isotope, a total of 23 groups of samples were collected as samples, including 14 groups of surface water, 4 groups of pore water and 5 groups of karst water; while 19 groups of samples collected to test hydrogen and oxygen isotope, including 8 groups of surface water, 5 groups of pore water and 6 groups of karst water.

2.2 Test methods

In this study, all groundwater samples were sampled and tested on site within 0.5 h before the end of the pumping experiment. 500 mL brown bottles were used for sampling, which were moistened and washed with distilled water and water to be sampled for 3 times respectively before the samples were loaded and caps were tightly screwed under water. Portable multi-parameter water quality analyzers (HI 9828, HANNA) were employed to determine pH, EC and other indicators of water bodies. Conventional chemical components (including K^+, Na^+, Ca^{2+}, Mg^{2+}, Cl^-, SO_4^{2-}, HCO_3^-, NO_3^-, TDS, H_2SiO_3) were determined in the laboratory of Henan Geological Engineering Investigation Institute: K^+, Na^+ were measured by flame atomic absorption spectrophotometer, Ca^{2+}, Mg^{2+}, Cl^- and HCO_3^- were measured by titration method, SO_4^{2-} was tested by turbidimetric method, NO_3^- by ultraviolet spectrophotometry, TDS by gravimetric method, and metasilicicic acid by silico-molybdenum yellow spectrophotometry. Hydrogen and oxygen isotopes were measured by DELTA V Advantage Isotope Ratio Mass Spectrometer of Wuhan Nuclide Technology Co., LTD. The charge balance errors of anions and cations in the collected samples were all within ±5%; and the testing errors of δD, $\delta^{18}O$-H_2O and $\delta^{34}S$-SO_4 are ±<0.5‰, ±<0.2‰ and ±<0.2‰, respectively.

3 Results

3.1 Hydrochemical characteristics

The hydrochemical results of different water samples are summarized in Table 1. As can be seen from Table 1, the pH value of the water bodied in the studied area ranged from 7.15 to 7.52. which was weakly alkaline in general. The TDS range of surface water in the studied area is 175.55–782.56 mg/L, and the TDS range of groundwater is 330.69–651.66 mg/L, both of which could be concluded as fresh water. Ranking from high to low, the average rates of concentration of the major cations in surface water were as follows: Ca^{2+}>Na^+>Mg^{2+}>K^+, with their respective contents as: 74.11±87.90, 23.49±45.39, 22.77±13.81, 7.19±6.24.; the average rates concentration of major anions were as follows: HCO_3^-> SO_4^{2-}> Cl^-> NO_3^-, with their respective contents as 199.01±115.26, 92.70±145.00, 63.47±201.34, 11.41±42.01. For ground water, ranking from high to low, the rates of the average concentrations of major cations were as follows: Ca^{2+}>Mg^{2+}>Na^+>K^+, with their respective contents as 96.41±38.02, 27.94±15.62, 19.43±14.15, 3.72±4.05; The rates of the average concentration of major anions were as follows: HCO_3^-> SO_4^{2-}> Cl^-> NO_3^-, with their respective contents as 325.76±54.42, 55.44±31.24, 47.45±112.07, 31.66±62.6. The saturation indices of calcite ad dolomite in the collected water samples, except

Table 1 Hydrochemical parameters and PHREEQC calculation results of water samples in the study area

Type	Number	pH	K^+	Na^+	Ca^{2+}	Mg^{2+}	Cl^-	SO_4^{2-}	HCO_3^-	NO_3^-	H_2SiO_3	TDS	Depth	SI-calcite	SI-dolomite
			Concentration（mg/L）										m		
Surface water	XF	7.15	5.45	19.35	46.53	26.13	20.74	73.20	223.62	6.86	20.12	310.64	0.00	−0.24	−0.38
	YL	7.19	3.70	4.07	43.09	10.45	15.95	23.65	139.00	4.86	7.44	175.55	0.00	−0.38	−1.02
	NT	7.22	12.00	17.44	67.21	26.13	25.52	61.28	290.10	12.70	24.49	368.10	0.00	0.09	0.11
	XS	7.25	9.12	15.10	86.17	29.26	35.10	83.16	314.27	16.55	5.36	432.17	0.00	0.24	0.35
	HS	7.28	9.38	16.10	39.64	15.68	38.29	13.50	181.31	1.30	5.89	225.28	0.00	−0.22	−0.50
	BS	7.30	11.17	68.88	89.62	27.17	82.95	203.80	229.66	34.81	3.30	634.39	0.00	0.13	0.07
	YH	7.33	6.56	42.06	151.66	36.58	118.05	237.70	271.96	53.42	16.48	782.56	0.00	0.42	0.56
	HTL	7.35	4.36	11.46	44.81	19.86	35.10	68.60	145.05	1.29	6.41	258.43	0.00	−0.22	−0.45
	MG	7.37	4.05	10.54	51.70	22.99	31.91	81.72	169.22	1.04	3.04	289.07	0.00	−0.08	−0.18
	LFS	7.40	8.74	13.55	44.81	19.86	38.29	48.26	169.22	1.09	1.24	259.60	0.00	−0.10	−0.21
	LT	7.45	3.51	9.33	65.49	17.77	41.48	87.04	145.05	6.00	0.20	303.63	0.00	0.03	−0.18
	LW	7.47	4.32	18.02	77.55	17.77	57.43	101.60	169.22	13.60	0.20	375.37	0.00	0.17	0.03
	YW	7.49	4.89	24.01	67.21	26.13	82.95	116.20	145.05	<0.88	0.20	394.33	0.00	0.05	0.03
	ZT	7.52	13.42	58.90	162.00	22.99	264.81	98.12	193.40	5.38	10.93	723.37	0.00	0.53	0.56
Pore water	ZK3	7.23	3.84	20.71	99.96	34.49	63.81	48.84	338.45	31.15	19.14	472.64	55.00	0.31	0.50
	ZK2	7.35	4.97	14.92	133.07	42.78	72.99	82.75	364.34	94.25	30.71	651.66	55.00	0.54	0.94
	ZK7	7.22	1.89	11.54	72.14	23.33	8.69	23.68	332.66	22.30	22.48	347.62	100.00	0.19	0.23
	ZK9	7.36	0.13	15.44	134.43	31.35	60.62	52.66	350.53	76.20	23.24	546.47	70.00	0.56	0.83
	ZK11	7.22	1.10	20.18	105.13	22.99	33.50	86.68	320.31	31.15	18.19	461.31	200.00	0.30	0.27
	ZK13	7.26	4.08	19.57	98.24	31.35	54.24	55.82	350.53	37.00	17.45	475.93	190.33	0.35	0.54
	ZK12	7.29	3.48	25.48	84.45	21.95	25.52	50.60	362.62	3.51	21.16	396.74	132.06	0.35	0.45
	ZK16	7.32	7.77	13.87	82.73	11.50	31.91	28.83	253.83	26.68	14.59	330.69	241.00	0.24	−0.04
Karstic water	SMH	7.30	3.94	26.90	98.56	43.56	159.53	63.60	229.66	43.50	21.98	554.76	300.00	0.20	0.38
	MZ-1	7.32	0.99	11.93	95.22	26.34	35.10	75.55	296.14	28.71	16.12	422.23	400.00	0.33	0.44
	ZK17	7.30	3.89	17.72	73.50	23.30	24.57	23.95	380.18	8.44	18.50	365.84	371.00	0.33	0.50
	PY-X	7.35	5.81	32.84	79.28	29.26	28.71	61.30	308.23	14.96	25.81	406.79	800.00	0.30	0.52
	PY-D	7.38	7.77	33.58	67.21	29.26	22.33	61.32	302.18	7.98	27.63	381.23	800.00	0.26	0.50
	ZK19	7.30	3.38	12.90	130.30	12.16	45.62	39.76	364.34	31.12	19.45	458.02	259.80	0.53	0.37
	DC-3	7.28	2.73	13.84	91.88	35.46	44.67	76.20	332.40	17.96	21.61	449.33	300.00	0.32	0.56

few in surface water samples were over saturated with the saturation index over 0. The highest sulfate concentrations were found in surface water samples (13.5–237.7 mg/L, mean 92.7 mg/L), followed by that in pore water (23.68–86.68 mg/L, mean 86.68mg/L), and the lowest sulfate concentrations were in karst water (23.95–76.2 mg/L, mean 57.38 mg/L).

As can be seen from Piper's triplex diagram (Fig. 3), the cations in the studied area are mainly located in the lower left corner, while the anions are mainly located in the upper end of the triangle and the lower left corner, showing a high degree of consistency. The surface water hydrochemical types are relatively complex (Table 2), and were divided into 6 types, which were dominated by HCO_3-Ca·Mg (42.86%) and HCO_3·SO_4-Ca·Mg (28.57%). The hydrochemical type of pore water is relatively simple with primary type of HCO_3-Ca·Mg (75%). For karst water hydrochemistry there are three types, mainly the HCO_3-Ca·Mg (71.43%) type.

The principal component analysis of groundwater indexes (Table 3 and Table 4) shows that SO_4^{2-} is moderately correlated with Mg^{2+} and Ca^{2+} 0.5–0.75), with the correlation coefficients being 0.628 and 0.509, respectively. The first components affecting groundwater hydrochemistry are Cl^-, NO_3^-, Ca^{2+}, Mg^{2+}, SO_4^{2-} and Na^+, with the respective loadings of 0.872, 0.850, 0.793, 0.723, 0.688 and 0.520. In general, Ca^{2+} and Mg^{2+} in groundwater mainly generated by the dissolution of silicates and carbonates in aquifers, while Cl^- and NO_3^- mostly comes from human activities (Jacob et al. 2023; Liu et al. 2020). In summary, the main factors affecting SO_4^{2-} and hydrochemical types in

the studied area were water-rock interaction and human production activities.

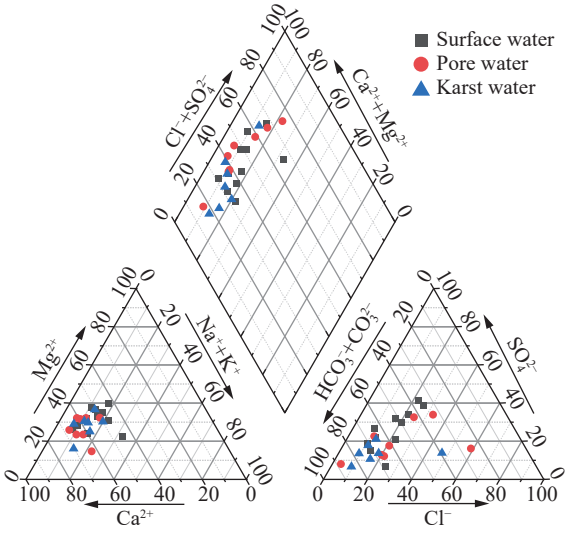

Fig. 3 Piper diagram showing the chemical compositions of the groundwater

Table 2 Hydrochemical types in Pingyu Mining area

Type	Hydrochemical type	Amount	Proportion (%)
Pore water	HCO_3—Ca·Mg	6	42.86
	HCO_3·SO_4—Ca·Mg	4	28.57
	SO_4·HCO_3—Ca	1	7.14
	SO_4·HCO_3—Ca·Na	1	7.14
	SO_4·HCO_3·Cl—Ca·Mg	1	7.14
	Cl—Ca	1	7.14
Pore water	HCO_3—Ca·Mg	6	75.00
	HCO_3—Ca	2	25.00
Karstic water	HCO_3—Ca·Mg	5	71.43
	HCO_3—Ca	1	14.29
	Cl·HCO_3—Ca·Mg	1	14.29

3.2 Isotope characteristics

Hydrogen and oxygen isotopes can be employed totrace the source of water recharge in the studied area. According to Fig. 4(a-c), the highest average value of δD (67‰–28‰) was found in surface water in the studied area, which was −50.88‰; the δD value of pore water ranges from −72‰ to 59‰ with the average value of −62.8‰; and the value of δD in karst water (−68‰–61‰) has the lowest average value of −64.17‰. In the studied area, the value of $\delta^{18}O$-H_2O in surface water is the highest, which ranges from −9.5‰ to −2.4‰ with an average value of −6.93‰; the value of $\delta^{18}O$-H_2O in pore water ranges from −10.2‰ to −8.5‰ with an average value of −9.02‰; and the value of $\delta^{18}O$-H_2O in karst water ranges from −9.7‰ to −8.6‰ with an average value of −9.15‰. $\delta^{34}S$-SO_4 values are all positive in the samples; the distribution of $\delta^{34}S$-SO_4 values in surface water is more dispersed (7.6‰–15.4‰), with an average value of 10.02‰; pore water contained a more concentrated distribution (11.7‰–15.1‰), with an average value of 12.73‰; in karst water, $\delta^{34}S$-SO_4 values ranged from 8.5‰ to 15.57‰ with an average value of 11.45‰. Comparatively, the value of $\delta^{34}S$-SO_4 in pore water is relatively the highest.

Since the studied area and Zhengzhou are adjacent to each other and shared similar the natural conditions of rainfall and temperature, the rainwater precipitationline of Zhengzhou area (Wu et al. 2022) can be selected to represent the local rainfall line of Pingyu mining area. The isotope test results of different water bodies in the mining area were fitted and shown in Fig. 4d. Most of the water samples collected in the studied area are located between the local rainfall line and the global rain-

Table 3 Correlation analysis table

	K^+	Na^+	Ca^{2+}	Mg^{2+}	Cl^-	SO_4^{2-}	HCO_3^-	NO_3^-	H_2SiO_3	TDS
K^+	1.000									
Na^+	0.237	1.000								
Ca^{2+}	−0.377	0.341	1.000							
Mg^{2+}	−0.116	0.342	0.277	1.000						
Cl^-	−0.136	0.474	0.548	0.629	1.000					
SO_4^{2-}	−0.266	0.386	**0.628**	**0.509**	0.347	1.000				
HCO_3^-	−0.285	−0.084	0.439	−0.036	−0.314	0.255	1.000			
NO_3^-	−0.297	0.253	0.886	0.513	0.604	**0.589**	0.311	1.000		
H_2SiO_3	0.079	0.336	0.390	0.438	0.143	0.494	0.378	0.446	1.000	
TDS	−0.306	0.450	0.923	0.602	0.705	**0.734**	0.337	0.930	0.513	1.000

Table 4 Eigenvectors of the 3 PCs

	1	2	3
K^+	−0.304	−0.130	**0.812**
Na^+	**0.520**	−0.023	0.617
Ca^{2+}	**0.793**	0.414	−0.226
Mg^{2+}	**0.723**	−0.063	0.229
Cl^-	**0.872**	−0.399	0.052
SO_4^{2-}	**0.688**	0.392	0.070
HCO_3^-	0.021	**0.902**	−0.228
NO_3^-	**0.850**	0.310	−0.158
H_2SiO_3	0.391	**0.628**	0.467
TDS	**0.936**	0.321	−0.045
Total	4.502	1.912	1.448
Variance percentage (%)	45.016	19.121	14.482
Accumulate%	45.016	64.137	78.620

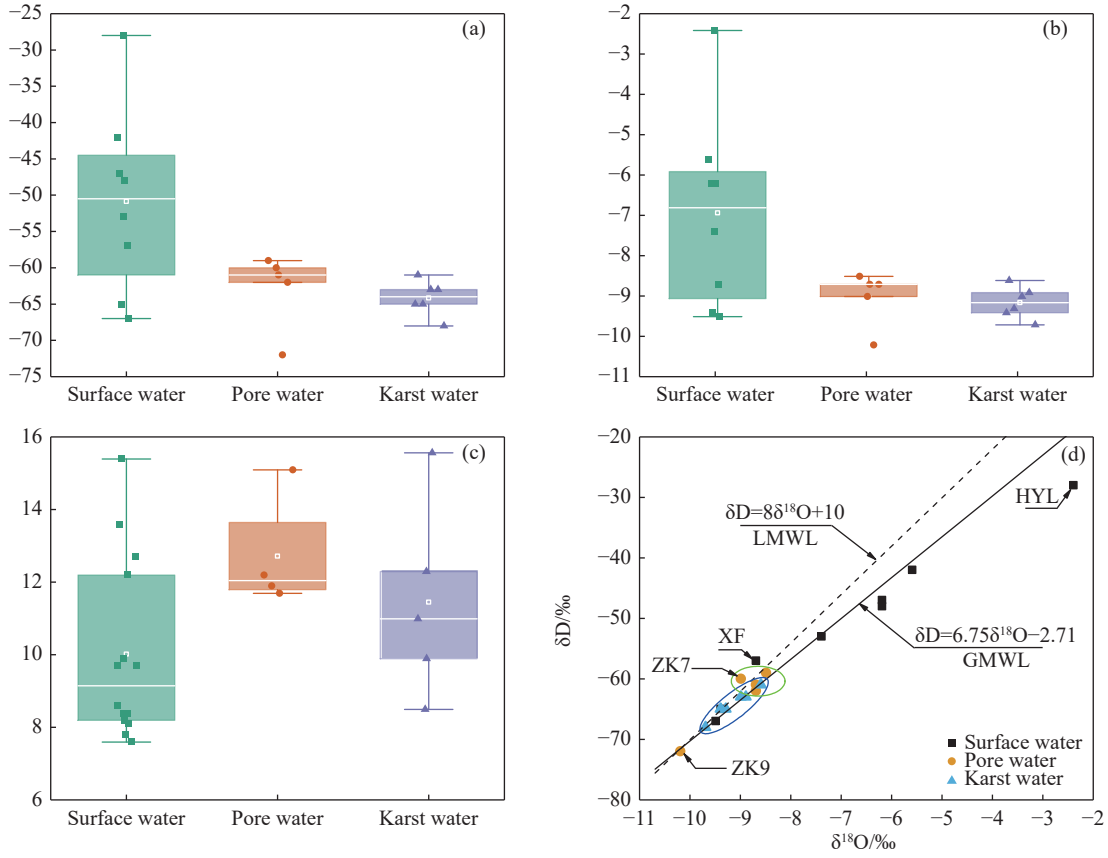

Fig. 4 Box plot of isotope in the Study Area ((a) D; (b) ^{18}O-H_2O; (c) ^{34}S- SO_4; (d) ^{18}O-H_2O versus D values of the water samples in reference to the GMWL and LMWL)

fall line, indicating that atmospheric precipitation is the primary recharge source of local water supply.

4 Discussion

4.1 Dissolution of carbonate and silicate rocks

The chemical composition of groundwater is governed by water-rock interactions (Zhang et al. 2021). Based on various ion ratio relationships, hydrochemical types of different origin can be qualitatively classified into different hydrochemistry genesis end-members. Gibbs diagram (Gibbs, 1970) is known as a valuable method of determining the source of the main chemical components in natural water by analyzing the relationship between Na^+, Ca^{2+}, Cl^-, HCO_3^- and TDS, which is capable of dividing the chemical components of

natural water into three end elements: Atmospheric precipitation, rock weathering, evaporation and crystallization. As is shown in Fig. 5a, except for sampling spot ZT, water samples in the study area are relatively concentrated, almost all of which fall in the category the rock weathering end element, signifying that the hydrochemistry of water bodies in the studied area is principally dominated by rock weathering effects. The ZT spot located in a sunken lake in the subsidence area formed by mine drainage and groundwater exposure to the surface. The water body at the ZT spot is basically static with evapotranspiration as its main drainage channel. Therefore, the water quality at this sampling point gradually fell under the controlled of evaporation and crystallization.

The molar ratio between Mg^{2+}/Na^{+} and Ca^{2+}/Na^{+} in groundwater is insusceptible to groundwater flow rate, dilution and evaporation, so the water-rock interaction process can be qualitatively identified by the Mg^{2+}/Na^{+} and Ca^{2+}/Na^{+} relationship (Huang et al. 2023). As Fig. 5b demonstrates, the water bodies in the study area mainly falls between carbonate and silicate end members, implying that the water body in this area is significantly affected by silicate and carbonate dissolution, whereas the dissolution of evaporite rocks (e.g. gypsum) has a lesser influence in the studied area.

Coal mining affects hydrogeochemical processes in mining areas (Cha et al. 2022; Acharya et al. 2020). Through the analysis of the interrelationships between multiple ions, it is possible to infer the hydrogeochemical processes occurring in aquifers (Zhang et al. 2021), which can then reveal the mechanism of sulfur cycle in groundwater. Drillings and previous research data show that siliceous masses or bands are widely present in karst aquifers in the studied area. Studies (Zou et al. 2022) that, under silicate-dominated environment, feldspar will react with carbonic acid to release HCO_3^-, Mg^{2+} and Ca^{2+} into water, thus the concentration of Na^+ and K^+ in the solution will also increase. Therefore, when the mEq ratio of $(Na^+ + K^+)/Cl^-$ is over 1, it is mainly the dissolution of rock salt that occurs in groundwater; when the ratio is below 1, it can be deduced that the dissolution of silicate also takes place. When it comes to Ca^{2+}, Mg^{2+}, HCO_3^- and SO_4^{2-} in groundwater, they are mainly derived from the weathering and dissolution of carbonates such as calcites and dolomites and evaporites such as gypsum (Jacob et al. 2023), and thus, when the $(Ca^{2+}+Mg^{2+})/(HCO_3^-+SO_4^{2-})$ mEq ratio is over 1, Ca^{2+} and Mg^{2+} in solution mainly come from the dissolution of carbonate.; if the ratio is below 1, it indicates that Ca^{2+} and Mg^{2+} are generated by the dissolution of silicates and evaporites. From Fig. 6a and Fig. 6b, it can be seen that most of the water bodies in the studied area are

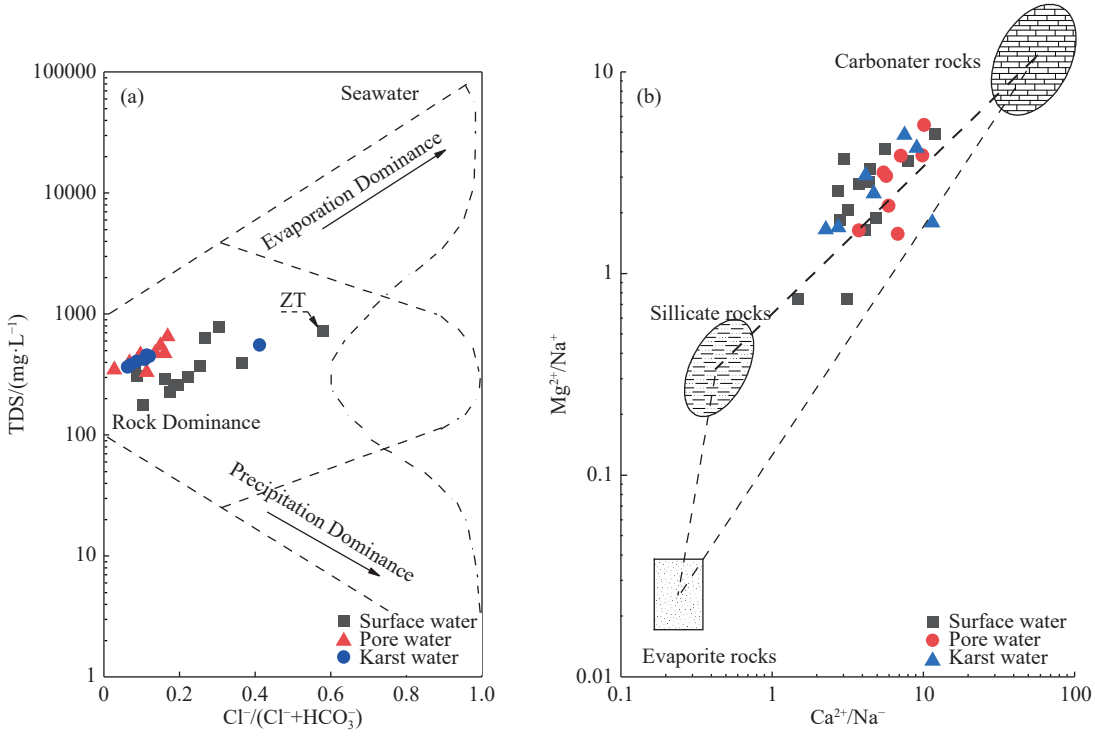

Fig. 5 End-element diagram of water chemistry in the study area ((a) Gibbs diagram; (b) Mg^{2+}/Na^{+} and Ca^{2+}/Na^{+}molar ratio end element diagram）

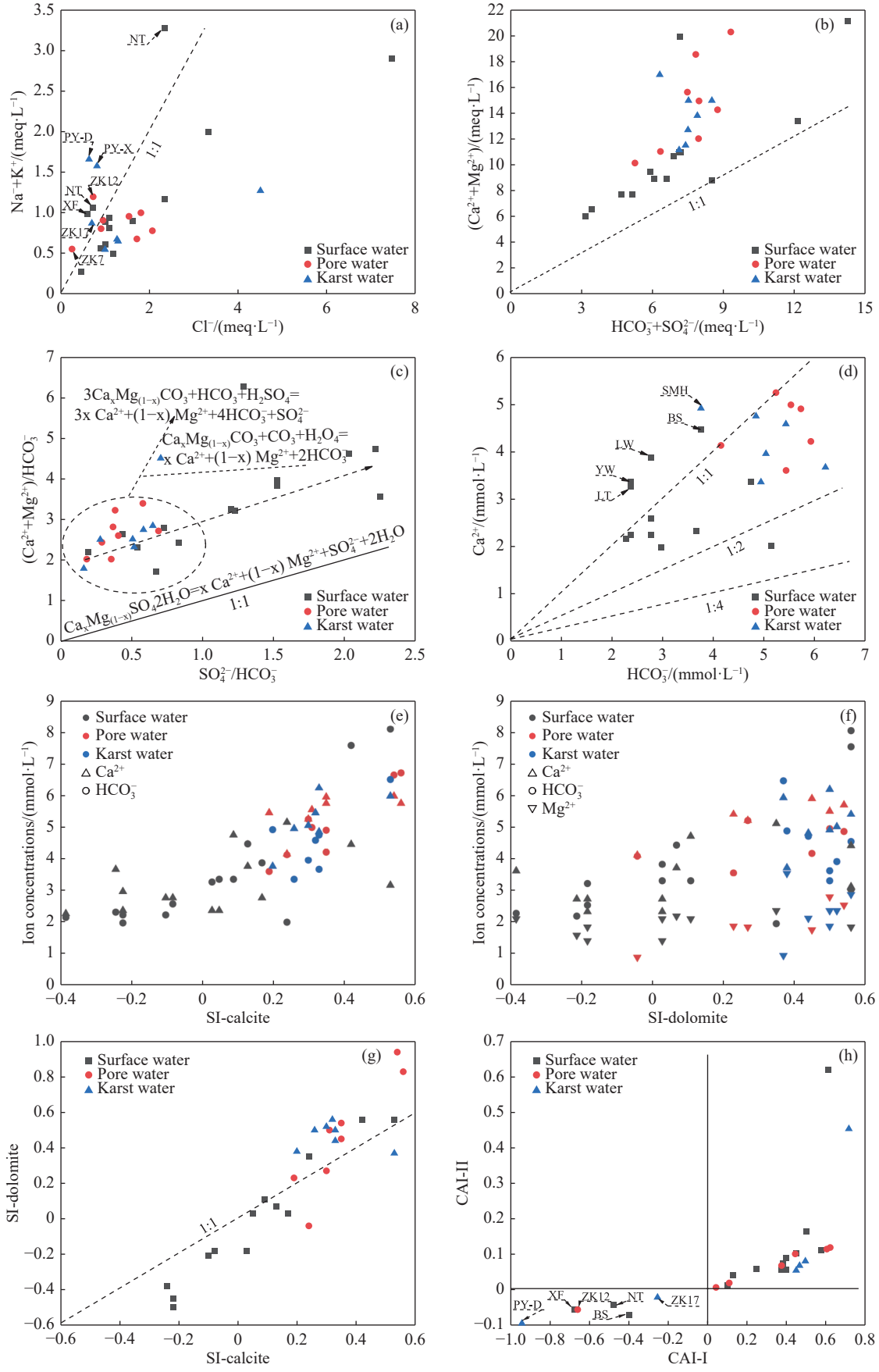

Fig. 6 Hydrochemical ion ratio in the study area

distributed below the equivalent ratio of Na^++K^+/Cl^- mgEq to 1:1, and the mg equivalent ratio of (Ca^{2+}+Mg^{2+})/(HCO_3^-+SO_4^{2-}) is much higher than 1, indicating that Ca^{2+} and Mg^{2+} in the area are mainly derived from the dissolution of carbonates. The dissolution of carbonates further promoted the dissolution of silicates, while the gypsum dissolution had relatively much smaller effect on SO_4^{2-} in water bodies this area.

4.2 Oxidation and dissolution of sulfide

If SO_4^{2-} in groundwater is mainly derived from the dissolved gypsum (Equation 1), then the molar ratio of (Ca^{2+}+ Mg^{2+})/ SO_4^{2-} should be 1. If the Ca^{2+} and HCO_3^- in groundwater primarily comes from the dissolution of calcite, then the molar ratio between Ca^{2+} and HCO_3^- should be 1:2 (Equation 2). Similarly, if dolomite is the only source of Ca^{2+}, Mg^{2+} and HCO_3^- in groundwater, the molar ratio between Ca^{2+} and HCO_3^- should be 1: 4 (Equation 3). The oxidation process of pyrite produces H_2SO_4, which is a strong carbonate weathering agent besides H_2CO_3. When the oxidation is also involved in karstification, the molar ratio of Ca^{2+}/HCO_3^- should be between 1:1 and 2:1 (Equation 4-6) (Jiang et al. 2022). As is shown in Fig. 6c and Fig. 6d, the water samples collected in the studied area are all found at the upper left of the (Ca^{2+}+Mg^{2+})/SO_4^{2-}=1 control line, signifying that the ratio of Ca^{2+}/HCO_3^- mole is between 1:1 and 2:1, that the (Ca^{2+}+Mg^{2+})/HCO_3^- mg equivalent ratio in groundwater increased with the increase of SO_4^{2-}/HCO_3^- mg equivalent ratio, and that SO_4^{2-} showed moderate correlation with Mg^{2+} and Ca^{2+} with correlation coefficients being 0.628 and 0.509, respectively. To summarize, the H_2SO_4 formed by the oxidation of pyrite was involved in the dissolution process in the studied area. In accord with Fig. 6e, Fig. 6f and Fig. 6g, calcite and dolomite in the water of the studied area are almost in a supersaturated state, and the concentrations of Ca^{2+}, Mg^{2+} and HCO_3^- raise with the increase of saturation degree. The saturation of dolomite in groundwater is significantly greater than that of calcite. These findings declared that the dissolution of dolomite in the studied area is accelerated by H_2SO_4 formed by the oxidation of pyrite. While there existed an indirect correlation between SO_4^{2-} and Mg^{2+} and Ca^{2+}, the oxidation and dissolution of pyrite in coal-bearing strata was the main source of SO_4^{2-} in the studied area.

$$\mathrm{Ca(x)Mg(1-x)SO_4 2H_2O} = \mathrm{xCa^{2+} + (1-x)Mg^{2+} + SO_4^{2-} + 2H_2O} \quad (1)$$

$$\mathrm{CaCO_3 + H_2O + CO_2 = Ca^{2+} + 2HCO_3^-} \quad (2)$$

$$\mathrm{CaMg(CO_3)_2 + 2H_2O + 2CO_2 = Ca^{2+} + Mg^{2+} + 4HCO_3^-} \quad (3)$$

$$\mathrm{2FeS_2 + 7O_2 + 2H_2O = 2FeSO_4 + 4H^+ + 2SO_4^{2-}} \quad (4)$$

$$\mathrm{CaMg(CO_3)_2 + H_2SO_4^2 = Ca^{2+} + Mg^{2+} + 2HCO_3^- + SO_4^{2-}} \quad (5)$$

$$\mathrm{2CaCO_3 + H_2SO_4 = 2Ca^{2+} + 2HCO_3^- + SO_4^{2-}} \quad (6)$$

4.3 Cation alternating adsorption

It can be seen from Fig. 6b and 6d that the (Ca^{2+}+ Mg^{2+})/(HCO_3^-+ SO_4^{2-}) mgEq ratio is well above 1:1, and sample from certain sampling points are located above the 1:1 molar ratio of Ca^{2+}/HCO_3^-, showing evident Ca^{2+} and Mg^{2+} surplus, which suggests that there could be reverse cation exchange in groundwater. The Schoeller index is applied here to assess the details of ion exchange between groundwater and aquifer medium. As is calculated using the Equation 1-2 below (milligram equivalent ratio). In general, Ca^{2+} and Mg^{2+} in groundwater will exchange Na^+ and K^+ in geotechnical particles on the surface of aquifer, which is a positive alternating effect, where the values of CAI-1 and CAI-Ⅱ are negative. Alternately, when Na^+ and K^+ increase in groundwater when supplemented by other water sources, Na^+ and K^+ will exchange Ca^{2+} and Mg^{2+} in the surface of geotechnical particles, which is a reverse alternating effect, where the values of CAI-1 and CAI-2 are both positive. The greater the absolute values of CAI-1 and CAI-2 are, the stronger the cation exchange is and the easier the cation exchange can occur.

$$\mathrm{CAI-1} = \frac{\mathrm{Cl^- - Na^+ - K^+}}{\mathrm{Cl^-}} \quad (7)$$

$$\mathrm{CAI-2} = \frac{\mathrm{Cl^- - Na^+ - K^+}}{\mathrm{SO_4^{2-} + HCO_3^- + CO_3^- + NO_3^-}} \quad (8)$$

As Fig. 6h demonstrates, most of the water samples fall in the first quadrant, and both values of CAI-1 and CAI-2 are positive, indicating that in most of the water samples in the studied area there exists a reverse cation exchange process, that is, Na^+ and K^+ from other sources exchange Ca^{2+} and Mg^{2+} out of the rock and soil matrix, causing the increase of Ca^{2+} and Mg^{2+} and meanwhile the decrease of Na^+ and K^+ in water bodies. It is worth noting that in Fig. 6a, still a small number of groundwater samples above the 1:1 mgEq ratio of (Na^++K^+)/Cl^-, but these points are located in the third quadrant of Fig. 6h, signifying that a small

number of water bodies in the studied area are still subject to positive cation exchange, which lead to the increase of Na^+ and K^+ but the decrease of Ca^{2+} and Mg^{2+} in the water bodies.

4.4 Sulfate isotopes source identification and microbial desulfation

The sources of SO_4^{2-} in water can be divided into three major categories: Atmospheric deposition, oxidation and dissolution of sulfide minerals and/or gypsum, and input of pollutants. Except for the bacterial sulfate reduction (BSR), significant fractionations generally do not occur in natural sulfates (Huang et al. 2023). The relationship between the ulfate $^{34}S\text{-}SO_4$ values and the SO_4^{2-} concentrates can, to a certain extent, be exploited to analyze the source of sulfate in water, and has been widely applied in the tracers for various sulfate sources in water, studying the hydrogeochemical processes (Wang et al. 2023; Mao et al. 2023).

Previous studies (Sabina et al. 2022; Zhou et al. 2016) have pointed out that, the values of $^{34}S\text{-}SO_4$ generated by common natural and anthropogenic sources are as shown in Fig. 7a. Combined with Fig. 7b and Fig. 7c, it can be concluded that the distribution of SO_4^{2-} concentration in surface water is relatively dispersed, with a minimum value of 13.5 mg/L and a maximum value of 237.7 mg/L. Except samples taken at points XF, NT, ZT and HS, the $^{34}S\text{-}SO_4$ value in surface water (7.6‰–9.9‰) is lower than that in groundwater, which is comparable to that of atmospheric precipitation (3‰–9‰), sewage water (8.7‰±2.4‰) and mine drainage (8.4‰±3.9), indicating that SO_4^{2-} in surface water in the studied area mainly derived from relatively complex sources and could be jointly affected by atmospheric precipitation, sewage and mine drainage at the same time. Larger values of $^{34}S\text{-}SO_4$ appeared at the sampling spots XF (12.2‰), NT (15.4‰) and ZT (12.7‰), located in the sedimentation lake in the periphery of the mine, with their respective SO_4^{2-} concentrations of 73.2 mg/L, 61.28 mg/L and 98.12 mg/L, appearing to have identical concentration of SO_4^{2-} (23.68 mg/L–86.68 mg/L) and distribution range of $^{34}S\text{-}SO_4$ (9.9‰–15.57‰) in groundwater. It can be concluded that SO_4^{2-} in the sedimentation lake is mainly supplied by groundwater.

Pore water and karst water in the studied area have the similar characteristics, taking form of low SO_4^{2-} concentration (23.95 mg/L–96.69 mg/L) and a high $\delta^{34}S\text{-}SO_4$ value (8.5‰–15.57‰), but the value was much lower than that in evaporite rock (20‰–35‰). In the process of coal min-

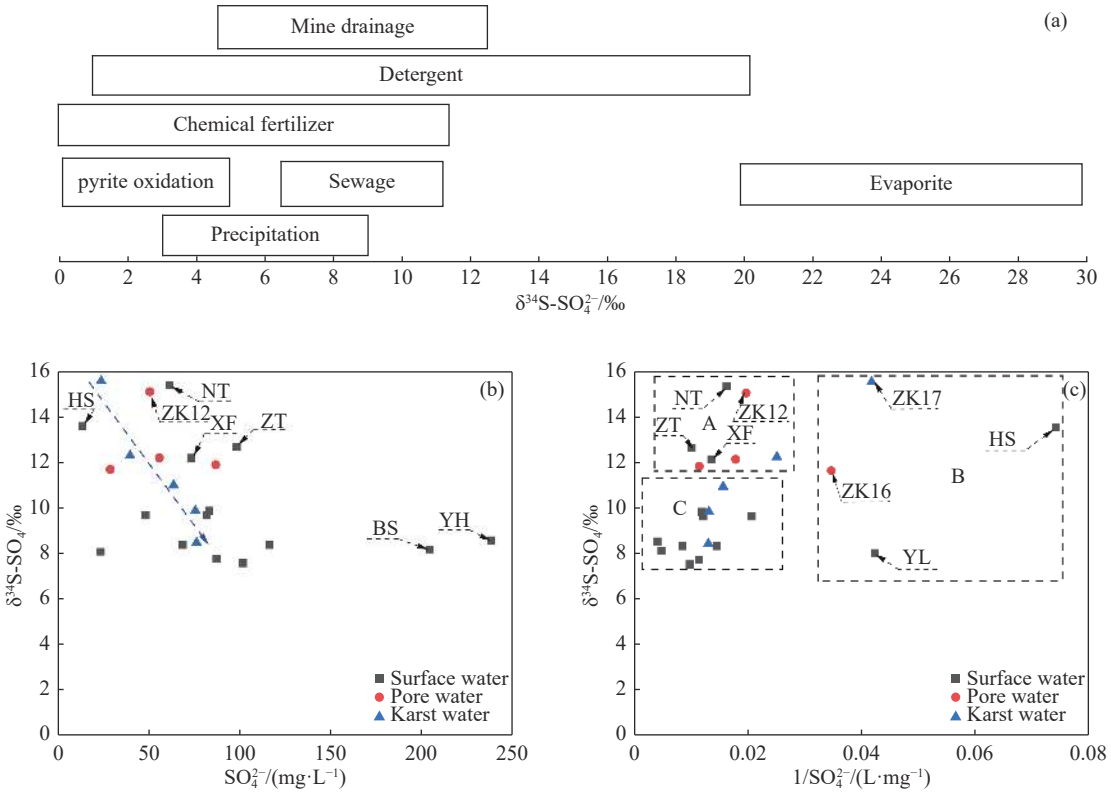

Fig. 7 Relationship between $^{34}S\text{-}SO_4$ and SO_4^{2-}

ing, the pyrite oxidation will form a large amount of mine water low in $^{34}S\text{-}SO_4$ value, which is then discharged to the surface, constantly mixing with surface water high in $^{34}S\text{-}SO_4$ value. Through the leaching and filtering effect of soil, the surface water is ceaselessly transformed into pore water, which then recharges the karst water through the fractions, fissures and holes at the bottom interface, resulting in the shared chemical characteristics of pore water and karst water. In accord with the condition of reduction, if oxidizable organic matter exists, bacteria can reduce SO_4^{2-} in groundwater to H_2S (Equation 7), causing large isotopic fractionation, bringing about the enrichment of $^{34}S\text{-}SO_4$ and the decrease of SO_4^{2-} concentration (Huang et al. 2023). As Fig. 8a exhibits, the significant negative correlation between $^{34}S\text{-}SO_4$ and SO_4^{2-} in karst water indicates that there may exist BSR fractionation process of $^{34}S\text{-}SO_4$ in undamaged deep karst water.

$$SO_4^{2-} + 2C + 2H_2O = H_2S + 2HCO_3^- \quad (9)$$

Based on the relationship between $^{34}S\text{-}SO_4$ value and $1/SO_4^{2-}$ in the water bodies of the studied area, this study divided the SO_4^{2-} source in the affected groundwater into three regions. As is shown in Fig. 7b, zone A showed high $^{34}S\text{-}SO_4$ value and high SO_4^{2-} concentration which is mainly composed of ZT and NT sampling points of sedimentation lake, XF sampling points of Happiness Lake and some groundwater sampling points, mainly demonstrating characteristics of mine water. Region B features high $^{34}S\text{-}SO_4$ value and low SO_4^{2-} concentration, which mainly consisted of river water sampling point HS, South-to-North Water Diversion point YL, pore water sampling point ZK16 and karst water sampling point ZK17, mainly representing the influence of SO_4^{2-} in atmospheric precipitation on the study area. Region C is characterized by low $^{34}S\text{-}SO_4$ value and high SO_4^{2-} concentration, which is made up of surface water sampling points and some karst water sampling points, majorly manifesting the influence of human activities and sulfide mineral oxidation on SO_4^{2-} in the water bodies.

4.5 Sulfur cycle processes

The mining activities severely damages the original stratigraphic structure, making the sulfides such as pyrite in the original closed environment fully expose to groundwater and air, thus accelerates the oxidation and weathering process of sulfide minerals in coal seam (Mao et al. 2023) and increases the SO_4^{2-} in groundwater. Intensive mining has completely changed the circulation process of groundwater in the studied area, forming a huge falling funnel-like landscape centered on the mine in the mining area and its surrounding subsidence area (Fig. 8). Karst water's discharge channel has been transformed from spring drainage to artificial mining drainage (Su et al. 2023). Large amounts of sulfate formed by the sulfides oxidation was discharged to the surface along with acidic mine water, mixing with the sulfate produced by human life and production in the sedimentation lake. The mixture then recharged groundwater aquifers rainfall infiltrated the ground and abandoned mines, in turn accelerating the dissolution process of carbonate and increasing TDS in groundwater. Meanwhile, the BSR process of sulfate still exists in the karst water system out of reach of mining impacts, which causes the accumulation of $^{34}S\text{-}SO_4$ and the continuous decrease of SO_4^{2-} in karst water.

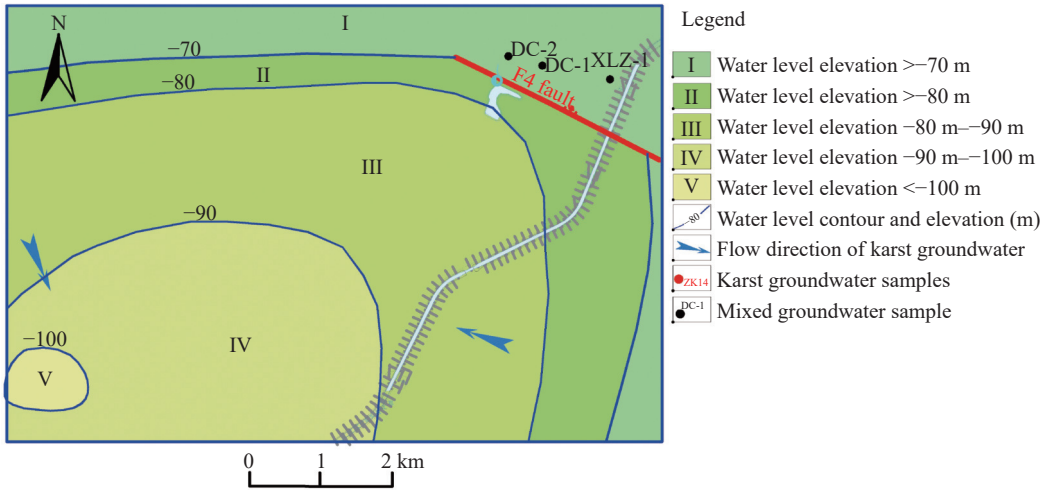

Fig. 8 Water level lines for karst water in mining areas and surrounding subsidence areas

5 Conclusions

(1) In the studied area, the water bodies in the subsidence zone of the mining area are weakly alkaline, and mainly recharged by atmospheric rainfall. The hydrochemical types of surface water in the area are dominated by HCO_3-Ca·Mg and HCO_3·SO_4-Ca·Mg, while the hydrochemical types of groundwater are primarily HCO_3-Ca·Mg, which are regulated by the oxidation and dissolution of carbonate rocks, silicate rocks and sulfides.

(2) Coal mining has severely damaged the original groundwater environment and changed the original hydrogeochemical process in the mining area and its surrounding subsidence area. Mine drainage accelerated the original water circulation around the mining area, resulting in the transformation of the groundwater environment from a reducing one to an oxidizing one. Sulfide minerals oxidized and dissolved on a large scale in the mining area produced large amounts of acidic mine water, accelerating the dissolution of carbonate rock (dolomite) and silicate rock. The hydrochemical processes in the studied area was also affected by positive and reversed cation exchange.

(3) The SO_4^{2-} in the groundwater of the sedimentation area of the mining area mainly was mostly generated by the sulfide minerals oxidation and dissolution and the wastewater formed by human activities. Sulfate formed by oxidizing and dissolving sulfide minerals was mixed with sulfate produced by production activities around the mining area, which contributed to the constant increase of TDS content in groundwater by continuously recharging the underground aquifer. In the deep, undisturbed karst water system of the subsidence area, there still existed BSR behavior, which led to the accumulation of ^{34}S- SO_4 and the decrease of SO_4^{2-} concentration.

Acknowledgements

This paper was supported by Geological Research Project of the Construction Management Bureau of the Middle Route of the South to North Water Diversion Project (ZXJ/HN/YW/GC-2020037)

References

Acharya BS, Kharel G. 2020. Acid mine drainage from coal mining in the United States - An overview. Journal of Hydrology, 588: 125061. DOI：10.1016/j.jhydrol.2020.125061.

Ansari MA, Noble J, Deodhar A, et al. 2020. Atmospheric factors controlling the stable isotopes ($\delta^{18}O$ and $\delta^{2}H$) of the Indian summer monsoon precipitation in a drying region of Eastern India. Journal of Hydrology, 584: 124636. DOI：10.1016/j.jhydrol.2020.124636.

Ágnes Ó, Juarez AF, Mariette S, et al. 2022. Sulfur and oxygen isotope constraints on sulfate sources and neutral rock drainage-related processes at a South African colliery. Science of the Total Environment, 846: 157178. DOI：10.1016/j.scitotenv.2022.157178.

Banks D, Boyce AJ, Burnside NM, et al. 2020. On the common occurrence of sulphate with elevated δ34S in European Mine waters: Sulphides, evaporites or seawater? International Journal of Coal Geology, 232: 103619. DOI：10.1016/j.coal.2020.103619.

Cha XF, Wu P, Li XX, et al. 2022. Karst hydrogeochemical characteristics and controlling factors of carlin-type gold mining area based on hydrochemistry and sulfur isotope. Environmental Science, 43(11): 5084−5095. (in Chinese) DOI：10.13227/j.hjkx.202112141.

David BW, Adrian JB, David B, et al. 2023. The occurrence of elevated $\delta^{34}S$ in dissolved sulfate in a multi-level coal mine water system, Glasgow, UK. International Journal of Coal Geology, 272: 104248. DOI：10.1016/j.coal.2023.104248.

Gibbs RJ. 1970. Mechanisms controlling world water chemistry. Science, 170(3962): 1088−1090. DOI：10.1126/science.170.3962.1088.

Huang PH, Zhang YN, Li YM, et al. 2023. A multiple isotope (S, H, O and C) approach to estimate sulfate increasing mechanism of groundwater in coal mine area. Science of the Total Environment, 900: 165852. DOI：10.1016/j.scitotenv.2023.165852.

Jacob A, Eric OA, Cynthia L, et al. 2023. Statistical and isotopic analysis of sources and evolution of groundwater. Physics And Chemistry Earth, Parts A/B/C, 129: 103337. DOI：10.1016/j.pce.2022.103337.

Jiang CL, Cheng LL, Li C, et al. 2022. A hydrochemical and multi-isotopic study of groundwater sulfate origin and contribution in the coal mining area. Ecotoxicology and Environ-

mental Safety, 248: 114286. DOI：10.1016/j.ecoenv.2022.114286.

Liu F, Wang S, Yeh TC J, et al. 2020. Using multivariate statistical techniques and geochemical modelling to identify factors controlling the evolution of groundwater chemistry in a typical transitional area between Taihang Mountains and North China Plain. Hydrological Processes, 34(8): 1888−1905. DOI：10.1002/hyp.13701.

Mao HR, Wang CY, Qu S, et al. 2023. Source and evolution of sulfate in the multi-layer groundwater system in an abandoned mine−insight from stable isotopes and Bayesian isotope mixing model. Science of the Total Environment, 859: 160368. DOI：10.1016/j.scitotenv.2022.160368.

Moya CE, Raiber M, Taulis M, et al. 2016. Using environmental isotopes and dissolved methane concentrations to constrain hydrochemical processes and inter-aquifer mixing in the Galilee and Eromanga Basins, Great Artesian Basin, Australia. Journal of Hydrology, 539: 304−318. DOI：10.1016/j.jhydrol.2016.05.016.

Pan GY, Zhang K, Wang PL. 2011. Using stable isotopes to determine the source of mine water supply - Taking Pingyu No. 1 Mine as an Example. Journal of Water Resources and Water Engineering, 22(06): 119−122. (in Chinese)

Qu S, Duan LM, Shi ZM, et al. 2022. Hydrochemical assessments and driving forces of groundwater quality and potential health risks of sulfate in a coalfield, northern Ordos Basin, China. Science of the Total Environment, 835: 155519. DOI：10.1016/j.scitotenv.2022.155519.

Ren K, Zeng J, Liang JP, et al. 2021. Impacts of acid mine drainage on Karst aquifers: Evidence from hydrogeochemistry, stable sulfur and oxygen isotopes. Science of the Total Environment, 761: 143223. DOI：10.1016/j.scitotenv.2020.143223.

Rinder T, Dietzel M, Stammeier JA, et al. 2020. Geochemistry of coal mine drainage, groundwater, and brines from the Ibbenbüren Mine, Germany: A coupled elemental-isotopic approach. Applied Geochemistry, 121: 104693. DOI：10.1016/j.apgeochem.2020.104693.

Sabina JK, Kinga S. 2022. Isotopic signature of anthropogenic sources of groundwater contamination with sulfate and its application to groundwater in a heavily urbanized and industrialized area (Upper Silesia, Poland). Journal of Hydrology, 612: 128255. DOI：10.1016/j.jhydrol.2022.128255.

Sahoo S, Khaoash S. 2020. Impact assessment of coal mining on groundwater chemistry and its quality from Brajrajnagar coal mining area using indexing models. Journal of Geochemical Exploration, 215: 106559. DOI：10.1016/j.gexplo.2020.106559.

Su C, Cheng ZS, Wei W, et al. 2018. Assessing groundwater availability and the response of the groundwater system to intensive exploitation in the North China Plain by analysis of long-term isotopic tracer data. Hydrogeology Journal, 26(5): 1401−1415. DOI：10.1007/s10040-018-1761-y.

Su HM, Zhang FW, Hou SY, et al. 2023. An analysis of groundwater circulation in the Pingyu mining area based on hydrochemical and isotopic characteristics of groundwater. Hydrogeology& Engineering Geology, 2023,50(05): 53−67. (in Chinese) DOI：10.16030/j.cnki.issn.1000-3665.202306010.

Tang H. 2011. Numerical simulation and prediction of Karst water dewatering flow in Pingyu 1st coal mine. Henan Province. M. S. thesis. Jiaozuo: Henan Polytechnic University. (in Chinese)

Tao M, Cheng WQ, Nie KM, et al. 2022. Life cycle assessment of underground coal mining in China. Science of the Total Environment, 805: 150231. DOI：10.1016/j.scitotenv.2021.150231.

Wang CY, Liao F, Wang GC, et al. 2023. Hydrogeochemical evolution induced by long-term mining activities in a multi-aquifer system in the mining area. Science of the Total Environment, 854: 158806. DOI：10.1016/j.scitotenv.2022.158806.

Wu XX, Chen FL, Zhou X, et al. 2022. Comparative analysis of precipitation isotopes and water vapor sources in Zhengzhou and Fuzhou. Environmental Chemistry, 41(1): 125−134. (in Chinese)

Zhang FY. 2017. Division and isotope correlation

study of groundwater aquifer group in Xuchang. Ground Water, 39(4): 40−41,111. (in Chinese) DOI：10.3969/j.issn.1004-1184.2017.04.012.

Zhang J, Chen LW, Hou XW, et al. 2021. Multi-isotopes and hydrochemistry combined to reveal the major factors affecting Carboniferous groundwater evolution in the Huaibei Coalfield, North China. Science of the Total Environment, 791: 148420. DOI：10.1016/j.scitotenv.2021.148420.

Zheng LG, Chen X, Dong XL, et al. 2019. Using $\delta^{34}S–SO_4$ and $\delta^{18}O–SO_4$ to trace the sources of sulfate in different types of surface water from the Linhuan coal-mining subsidence area of Huaibei, China. Ecotoxicology and Environmental Safety, 181: 231−240. DOI：10.1016/j.ecoenv.2019.06.001.

Zhou JW, Zhang YP, Zhou AG, et al. 2016. Application of hydrochemistry and stable isotopes ($\delta^{34}S$, $\delta^{18}O$ and $\delta^{37}Cl$) to trace natural and anthropogenic influences on the quality of groundwater in the piedmont region, Shijiazhuang, China. Applied Geochemistry, 71: 63−72. DOI：10.1016/j.apgeochem.2016.05.018.

Zou S, Zhang D, Li XQ, et al. 2022. Sources and pollution pathways of deep groundwater sulfate underneath the Piedmont Plain in the North Henan Province. Earth Science, 47(2): 700−716. (in Chinese)